Maximum Proton Energy above 85 MeV from the Relativistic Interaction of Laser Pulses with Micrometer Thick CH2 Targets

F. Wagner,[1,2,*] O. Deppert,[3] C. Brabetz,[1] P. Fiala,[3] A. Kleinschmidt,[3] P. Poth,[3] V. A. Schanz,[3] A. Tebartz,[3]
B. Zielbauer,[1] M. Roth,[3] T. Stöhlker,[1,2] and V. Bagnoud[1,2]

[1]*GSI Helmholtzzentrum für Schwerionenforschung GmbH, Planckstraße 1, 64291 Darmstadt, Germany*
[2]*Helmholtz Institut Jena, Fröbelstieg 3, 07743 Jena, Germany*
[3]*Institut für Kernphysik, Technische Universität Darmstadt, Schlossgartenstraße 9, 64289 Darmstadt, Germany*
(Received 1 December 2015; published 19 May 2016)

We present a study of laser-driven ion acceleration with micrometer and submicrometer thick plastic targets. Using laser pulses with high temporal contrast and an intensity of the order of 10^{20} W/cm^2 we observe proton beams with cutoff energies in excess of 85 MeV and particle numbers of 10^9 in an energy bin of 1 MeV around this maximum. We show that applying the target normal sheath acceleration mechanism with submicrometer thick targets is a very robust way to achieve such high ion energies and particle fluxes. Our results are backed with 2D particle in cell simulations furthermore predicting cutoff energies above 200 MeV for acceleration based on relativistic transparency. This predicted regime can be probed after a few technically feasible adjustments of the laser and target parameters.

Laser-driven ion acceleration research received renewed interest after the experimental demonstration of target normal sheath acceleration (TNSA) 15 years ago [1]. However, despite numerous efforts to optimize laser and target conditions in order to achieve higher maximum ion energies, it was not until recently that the initially observed maximum proton energy of 58 MeV [1] could be exceeded [2]. At the same time several proposed applications for laser-driven ions, e.g., radiation therapy [3], are very demanding especially with respect to particle energy and average flux. It has been shown that the energy maximum of ions accelerated via TNSA can be enhanced by using thinner targets with thicknesses in the range of a few hundred nanometers to a few micrometers [4–7], while the thicknesses that are typically used are of the order of tens of micrometers.

However, while these investigations of target thickness effects were restricted to certain ultrashort pulse Ti:sapphire lasers that could fulfill the tough temporal contrast requirements, the comparison of many experiments carried out at different laser systems around the world shows that the highest maximum proton energies are achieved with laser systems that use Nd:glass amplifiers to provide high laser energy (> 100 J) in relatively long pulses (100 fs to 1 ps) (see Table 2 of Ref. [2]).

Furthermore, two alternative acceleration mechanisms based on ultrathin targets have been proposed with a view to reach the high maximum ion energies requested for applications: laser breakout afterburner (BOA) [8] and radiation pressure acceleration (RPA) [9,10]. The BOA mechanism is based on the fact that for matched laser and target conditions the target becomes relativistically transparent while interacting with the laser pulse. During this

phase a higher conversion efficiency of laser energy to the accelerated ions is expected leading to higher maximum ion energies. Therefore, for a given intensity, a pronounced optimum target thickness is a clear feature of this mechanism as pointed out in Ref. [11]. Experimentally, an essential increase of maximum energy and conversion efficiency could be demonstrated for accelerated carbon ions [12] and the first promising results have been obtained for deuterons and protons [13]. The RPA mechanism is fundamentally different from the BOA mechanism requiring that the target stays opaque while interacting with the laser pulse. Apart from this RPA also features a sharp optimum target thickness, which is predicted to be on the order of a few tens of nanometers for intensities around 10^{20} W/cm^2 as used in this experiment. These preconditions set high requirements on the laser and target properties, which is why apart from the first proof-of-principle experiments no enhancement of maximum proton energies could be demonstrated yet.

In this article we investigate laser-driven ion acceleration with micrometer and submicrometer thick plastic targets and relatively long (~0.5 ps) laser pulses with high energy (~200 J) obtained from a combined Ti:sapphire Nd:glass laser system. We show that TNSA with submicrometer thick targets is a robust approach to achieve high ion energies in excess of 70 MeV that is much less sensitive to fluctuations of laser and target parameters than alternative mechanisms.

The experimental results were obtained with the PHELIX (Petawatt High Energy Laser for heavy Ion eXperiments) laser [14] at the GSI Helmholtzzentrum für Schwerionenforschung GmbH in Darmstadt, Germany. The laser delivered an energy of 160–200 J after compression to
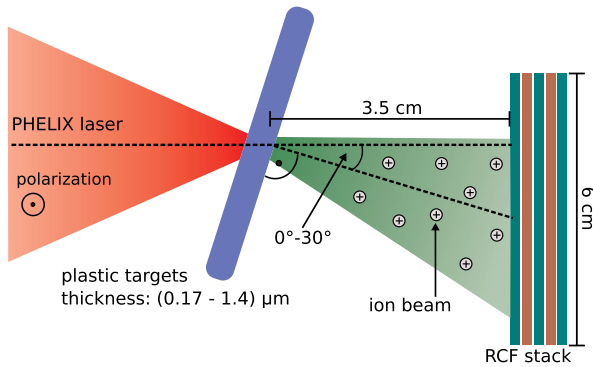
FIG. 1.   Experimental setup: the laser pulse impacts the target under different angles between 0° and 30°. The accelerated protons are detected with a stack of radiochromic film.
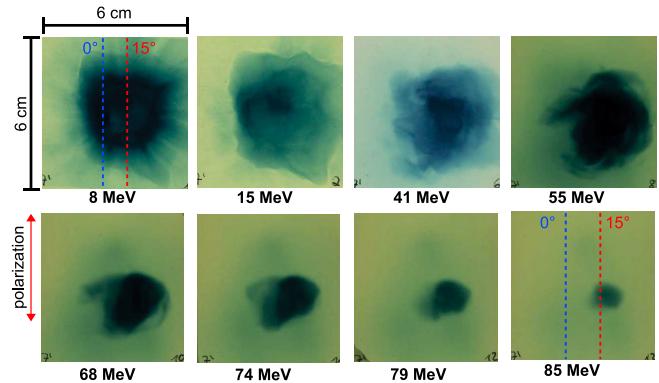

FIG. 2.   Selection of radiochromic film from a shot on a 900 nm thick plastic target (raw data). The energy of the protons that are fully stopped in the particular foil is written underneath each layer. For the first and the last layer the two angles corresponding to the laser axis (0°) and the target normal (15°) are illustrated by dashed lines.

500–800 fs. These pulses were focused onto the target under different angles of incidence ranging from 0° to 30° using an $f/1.7$ focusing parabola (Fig. 1). The laser focus was characterized at low energy showing a $4 \pm 0.5\ \mu m$ (FWHM) focal spot comprising 30% of the total energy. In addition the focal spot was monitored during the shot using a leak in the laser chain and a 16-bit CMOS camera to account for on-shot aberrations and improve the assessment on the laser intensity. This leads to an estimate of the mean on-target intensity of 0.7–2.6×10^{20} W/cm^2.

We used flat polymethylpentene targets with thicknesses ranging from 165 to 1400 nm as well as 4 μm thick gold targets. Thanks to an ultrahigh temporal contrast, front-end [15,16] preionization of the targets could be prevented up to 100 ps before the impact of the main pulse, which has been confirmed in former experiments [17,18]. A pulse trace which is valid for this experiment is given in Fig. 5 of Ref. [15].

Our main diagnostic relied on radiochromic film (RCF) in a stack configuration, which provides information on the spectrum as well as the spatial distribution of the accelerated proton beams [19]. Each RCF stack consisted of up to 15 radiochromic films. The three different types of Gafchromic film, HD-42, MD-V2, and EBT3, were used, which were calibrated prior to this experiment by our group. By using copper and nickel foils as intermediate layers in the stack the total detectable energy range was extended to 85 MeV. The maximum proton energies retrieved from the last colored RCF layer were additionally confirmed by measuring the nuclear activation of the metal foils as described in Ref. [20].

Figure 2 shows a selection of RCF layers exposed to the ion beam accelerated from a 900 nm thick plastic target. The angle of incidence was 15° for this shot, which enabled us to distinguish between ions accelerated in the target normal direction and the laser forward direction, respectively. As we described in Ref. [18], the direction of the accelerated beam allows for discrimination between different acceleration mechanisms. In this case the center of the

imprint on the RCF corresponds to the target normal direction, which is an indication for the TNSA mechanism. The coloring is present up to the last layer of our stack that detects only protons with an energy of 85 MeV or higher. Using the RCF data the spectra for the accelerated proton beams can be retrieved. This can be done in two different ways: first, by adjusting the free parameters of a test function for the spectrum to fit the calculated to the measured energy deposition in the RCF as described in Ref. [18] (in the following referred to as the first method) or, second, by stepwise unfolding the RCF response from the measured dose [21] (in the following referred to as the second method). Both methods were applied to our RCF data and the results are shown in Fig. 3. The uncertainties of these methods, which are mainly due to an imprecise differentiation between the signal and the background, are
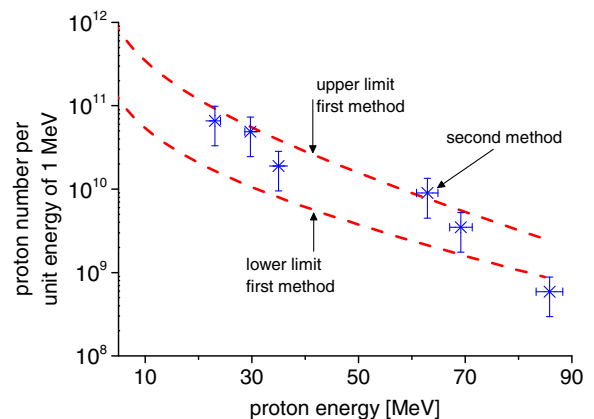

FIG. 3.   Proton spectrum from a shot on a 900 nm thick plastic target. The red dashed lines are obtained from the first method of analysis (see the text for explanation) and show an upper and a lower limit for the particle spectrum. The blue asterisks are obtained from the second method.
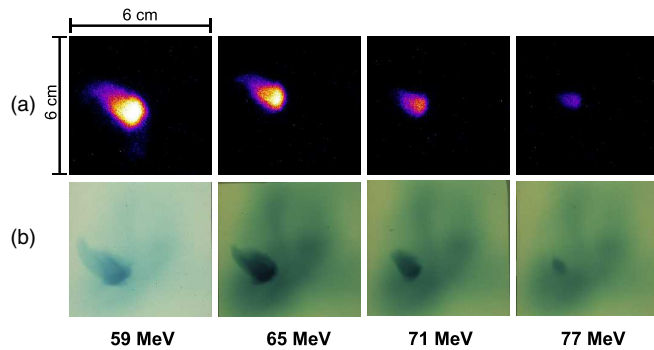
FIG. 4.   Proton beam profiles obtained from a shot on a 170 nm thick plastic target (a) from measurement of the copper activation. (b) Beam profiles on selected RCF layers (raw data).
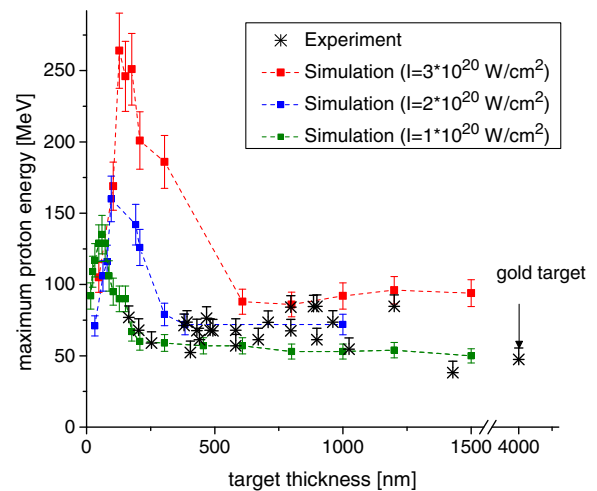

FIG. 5.   Maximum proton energy detected from the range of the protons in the RCF stack for different target thicknesses. The black asterisks are the measured energy maxima (each asterisk corresponds to one shot). The blue, red, and green squares are obtained from 2D-PIC simulations for different maximum laser intensities.

taken into account by showing an upper limit and a lower limit for the spectral function in the case of the first method and by using error bars for the second method. The particle number is monotonically decreasing for higher energies, which is typical for ions accelerated via TNSA [2,22]. At an energy of 85 MeV, particle numbers in an energy bin of 1 MeV are on the order of 10^9. This maximum energy is nearly 50% higher than the value observed by Snavely *et al.* [1]. The conversion efficiency of the laser energy entering the target chamber into protons with an energy above 4 MeV can be calculated by integrating the spectrum, resulting in a value of $7\% \pm 3\%$.

The measured energy maxima are additionally confirmed by measuring the nuclear activation of the copper foils that are used as intermediate layers in the RCF stack as described in Ref. [20]. Protons with energies above 4 MeV cause a transmutation of copper into an unstable zinc isotope that decays by emitting a positron. This radiation is detected shortly after the shot using image plates. As an example, the results from a shot on a 170 nm thick plastic target are shown in Fig. 4. The beam imprints on the radiochromic film resemble those obtained by imaging the nuclear activation. Furthermore, both techniques yield the same maximum proton energy, which is 77 MeV for this shot. Besides the nearly circular imprint of the proton beam an additional coloring can be seen on the RCF layers, which we observed for several shots. Since this feature is not present in the nuclear activation images it is clearly not caused by a proton beam. One possible source is fast electrons that are also detected in the RCF but do not trigger nuclear activation.

In the experimental campaign a total of 33 laser shots were taken. For different angles of incidence from 0° to 30° we always observed proton beams in the target normal direction, which is a sign for the TNSA mechanism. The energy maxima obtained from the range of the proton beams in the RCF stack are shown in Fig. 5 as a function of target thickness. Since we did not observe any difference regarding maximum proton energies for the different angles of incidence, as also reported in Ref. [23], we do not

distinguish between these angles in the graph. The energy maxima are clearly independent of the target thickness. The average maximum proton energy is 70 MeV and for several shots the last layer of our RCF stack was colored, which demonstrates maximum proton energies of 85 MeV or higher. These higher maximum energies compared to those we got in an earlier experiment under similar conditions [18] (~35 MeV) are attributed to reduced on-shot aberrations of the laser beam leading to a higher actual intensity. The fluctuations of the measured energies can be ascribed to a variation of the laser intensity as described above. These constant energy maxima for different target thicknesses are an additional sign for the TNSA mechanism instead of the BOA mechanism since the latter features a sharp optimum thickness as described in Refs. [11,18]. We would like to point out here that these results do not contradict the above mentioned findings of increased proton energies for thinner targets. For TNSA, such an effect is expected only if the thickness varies from a value that is large compared to the focus diameter to a value on the order of this diameter, which is typically a variation from about 1 to 100 μm. This can also be seen in Fig. 40 of Ref. [2], which summarizes the results obtained at different laser systems. In addition, we would like to mention that in spite of our initial conditions, which are not optimized for alternative mechanisms other than the TNSA or BOA mechanisms, the laser and plasma parameters are changed during the interaction and a contribution of other mechanisms such as RPA cannot be definitely excluded. The above described primary characteristics of the proton beam are in favor of the TNSA mechanism but secondary features of such contributions (e.g., modulations

of the spectrum) might be present in the proton beam that are not resolved by our detection method and remain to be investigated.

Particle in cell (PIC) simulations provide further insight into the acceleration mechanism. For this purpose 2D simulations were carried out with the PIC code EPOCH [24]. The simulation box was $240 \times 60 \ \mu m^2$ in size with a spatial grid resolution of $8 \times 20 \ nm^2$, a temporal resolution of 0.02 fs per time step, and open boundary conditions for particles and fields. The spatial as well as the temporal laser envelope were set to be Gaussian profiles. The target was modeled as a mixture of fully ionized hydrogen and carbon with $6 \times 10^{21} \ C_6H_{12}$ constituents per cm^3. Within the target boundaries 100 macroparticles per cell were used for protons, 50 for carbon ions, and 400 for electrons. The laser was focused onto the target surface located 20 μm from the left boundary, resulting in a focal spot diameter of 4.5 μm (FWHM). The small transversal size of the target was used to reach a viable computing time (22 500 CPU hours per simulation). However, we performed a few representative simulations with increased transversal dimensions to estimate the effect of mass limitation on the energy maxima, which was less than $\pm 10\%$ for our laser and target configuration. The maximum proton energies were evaluated at an instant of 1.4 ps after the impact of the peak of the 500 fs (FWHM) long laser pulse at the target surface. At this time the maximum proton energy was still rising slightly but this effect, which can mostly be attributed to numerical artifacts, was estimated to be less than 5% by looking at the evolution of the energy maxima for a few representative simulations. To take into account the aforementioned fluctuations of the laser intensity, simulations were done with two different intensities representing an upper and a lower limit, respectively, and an intermediate intensity. The results of the simulations are also shown in Fig. 5. For the thicker targets the measured data agree very well with the simulation. For very thin targets the simulations show a peak that is at considerably higher energies. This peak, the position of which depends on the laser intensity, can be ascribed to an enhanced acceleration during a phase of relativistic transparency as expected for the BOA mechanism [8]. This is confirmed by Fig. 6 showing that a 100 nm thick target irradiated with a peak intensity of 3×10^{20} W/cm^2 is transparent 100 fs before the impact of maximum intensity while a 1000 nm thick target stays opaque.

Even though the simulated peaks are at lower target thicknesses than the thinnest targets used in the experiment one might still have expected an enhanced maximum proton energy for targets below 400 nm as predicted by the rising slope of the simulated peak. One possible explanation for the absence of these enhanced proton energies is that for the few shots on the thinnest targets the laser intensity happened to be at the lower limit of the expected values, shifting the peak to even lower
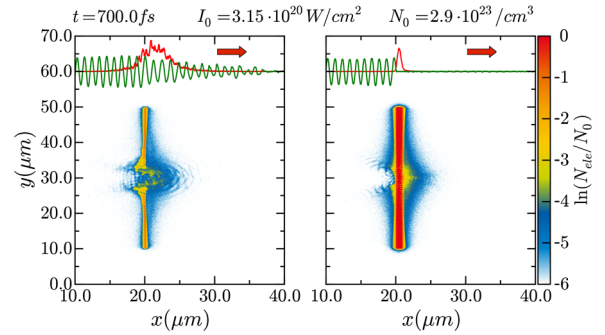

FIG. 6. Results from 2D-PIC simulations for plastic targets with thicknesses of 100 nm (left) and 1 μm (right). The coloring illustrates the electron density for a simulation time of 700 fs (the pulse maximum impacts the target surface at 800 fs). The 100 nm thick target is transparent for the laser (the lineout of the electric field of the laser at the target center is shown by the green line) while the laser pulse is stopped at the target surface for the 1 μm thick target. The arrow shows the laser propagation direction.

thicknesses. Another reason might be the imperfect temporal shape of the laser pulse. Even though the level of amplified spontaneous emission was below the ionization threshold of the targets, the slowly rising slope of the pulse leads to preionization of the target tens of picoseconds before the impact of the pulse maximum, which could be an issue for the thinnest targets [15]. Both options can be investigated in future experiments: first, by taking more shots on the thinner targets to gain more statistics with different laser intensities, second, by increasing the picosecond contrast by using one or two plasma mirrors, and, third, by using different target materials like diamondlike carbon, which can be manufactured at thicknesses far below 200 nm with still sufficient surface quality unlike the spin-coated polymethylpentene targets used in our experiment.

In conclusion our experimental realization of proton energies of 85 MeV with high particle numbers is a major step forward for laser-driven ion acceleration. We have shown that the use of submicrometer thick targets and acceleration via the TNSA mechanism is a very robust way to achieve proton energies in excess of 70 MeV. Our simulations, which are in good agreement with the experimental results, also suggest a way to achieve energy maxima in excess of 200 MeV, namely, by further increasing the temporal contrast, and by using target thicknesses of the order of 100 nm.

*f.wagner@gsi.de

[1] R. A. Snavely, M. H. Key, S. P. Hatchett, T. E. Cowan, M. Roth, T. W. Phillips, M. A. Stoyer, E. A. Henry, T. C. Sangster, M. S. Singh, S. C. Wilks, A. MacKinnon, A. Offenberger, D. M. Pennington, K. Yasuike, A. B. Langdon, B. F. Lasinski, J. Johnson, M. D. Perry, and E. M. Campbell, Phys. Rev. Lett. **85**, 2945 (2000).

[2] H. Daido, M. Nishiuchi, and A. Pirozhkov, Rep. Prog. Phys. **75**, 056401 (2012).

[3] S. V. Bulanov and V. S. Khoroshkov, Plasma Phys. Rep. **28**, 453 (2002).

[4] D. Neely, P. Foster, A. Robinson, F. Lindau, O. Lundh, A. Persson, C.-G. Wahlström, and P. McKenna, Appl. Phys. Lett. **89**, 021502 (2006).

[5] M. Kaluza, J. Schreiber, M. I. K. Santala, G. D. Tsakiris, K. Eidmann, J. Meyer-ter-Vehn, and K. J. Witte, Phys. Rev. Lett. **93**, 045003 (2004).

[6] A. J. Mackinnon, Y. Sentoku, P. K. Patel, D. W. Price, S. Hatchett, M. H. Key, C. Andersen, R. Snavely, and R. R. Freeman, Phys. Rev. Lett. **88**, 215006 (2002).

[7] J. Fuchs, P. Antici, E. dHumires, E. Lefebvre, M. Borghesi, E. Brambrink, C. A. Cecchetti, M. Kaluza, V. Malka, and M. Manclossi, Nat. Phys. **2**, 48 (2006).

[8] L. Yin, B. J. Albright, B. M. Hegelich, K. J. Bowers, K. A. Flippo, T. J. T. Kwan, and J. C. Fernández, Phys. Plasmas **14**, 056706 (2007).

[9] T. Esirkepov, M. Borghesi, S. V. Bulanov, G. Mourou, and T. Tajima, Phys. Rev. Lett. **92**, 175003 (2004).

[10] A. Henig, S. Steinke, M. Schnürer, T. Sokollik, R. Hörlein, D. Kiefer, D. Jung, J. Schreiber, B. M. Hegelich, X. Q. Yan, J. Meyer-ter-Vehn, T. Tajima, P. V. Nickles, W. Sandner, and D. Habs, Phys. Rev. Lett. **103**, 245003 (2009).

[11] L. Yin, B. J. Albright, D. Jung, R. C. Shah, S. Palaniyappan, K. J. Bowers, A. Henig, J. C. Fernández, and B. M. Hegelich, Phys. Plasmas **18**, 063103 (2011).

[12] D. Jung, L. Yin, B. J. Albright, D. C. Gautier, S. Letzring, B. Dromey, M. Yeung, R. Hörlein, R. Shah, S. Palaniyappan, K. Allinger, J. Schreiber, K. J. Bowers, H. C. Wu, J. C. Fernández, D. Habs, and B. M. Hegelich, New J. Phys. **15**, 123035 (2013).

[13] M. Roth *et al.*, Phys. Rev. Lett. **110**, 044802 (2013).

[14] V. Bagnoud *et al.*, Appl. Phys. B **100**, 137 (2010).

[15] F. Wagner, C. P. Joao, J. Fils, T. Gottschall, J. Hein, J. Körner, J. Limpert, M. Roth, T. Stöhlker, and V. Bagnoud, Appl. Phys. B **116**, 429 (2014).

[16] C. P. Joao, F. Wagner, J. Körner, J. Hein, T. Gottschall, J. Limpert, and V. Bagnoud, Appl. Phys. B **118**, 401 (2015).

[17] F. Wagner, S. Bedacht, A. Ortner, M. Roth, A. Tauschwitz, B. Zielbauer, and V. Bagnoud, Opt. Express **22**, 29505 (2014).

[18] F. Wagner, S. Bedacht, V. Bagnoud, O. Deppert, S. Geschwind, R. Jaeger, A. Ortner, A. Tebartz, B. Zielbauer, D. H. H. Hoffmann, and M. Roth, Phys. Plasmas **22**, 063110 (2015).

[19] F. Nürnberg, M. Schollmeier, E. Brambrink, A. Blazevic, D. C. Carroll, K. Flippo, D. C. Gautier, M. Geissel, K. Harres, B. M. Hegelich, O. Lundh, K. Markey, P. McKenna, D. Neely, J. Schreiber, and M. Roth, Rev. Sci. Instrum. **80**, 033301 (2009).

[20] M. M. Günther, A. Britz, R. J. Clarke, K. Harres, G. Hoffmeister, F. Nürnberg, A. Otten, A. Pelka, M. Roth, and K. Vogt, Rev. Sci. Instrum. **84**, 073305 (2013).

[21] M. Schollmeier, M. Geissel, A. B. Sefkow, and K. A. Flippo, Rev. Sci. Instrum. **85**, 043305 (2014).

[22] A. Macchi, M. Borghesi, and M. Passoni, Rev. Mod. Phys. **85**, 751 (2013).

[23] R. J. Gray, X. H. Yuan, D. C. Carroll, C. M. Brenner, M. Coury, M. N. Quinn, O. Tresca, B. Zielbauer, B. Aurand, V. Bagnoud, J. Fils, T. Kuehl, X. X. Lin, C. Li, Y. T. Li, M. Roth, D. Neely, and P. McKenna, Appl. Phys. Lett. **99**, 171502 (2011).

[24] T. D. Arber, K. Bennett, C. S. Brady, A. Lawrence-Douglas, M. G. Ramsay, N. J. Sircombe, P. Gillies, R. G. Evans, H. Schmitz, A. R. Bell, and C. P. Ridgers, Plasma Phys. Controlled Fusion **57**, 113001 (2015).